Supporting Information

Going hi-res in bulk: flowless multiangle dynamic light scattering for detection on asymmetric flow field flow fractionation.

Authors: Lavinia Rita Doveri,[1,a] Giorgia Dal Pan,[1,a] Giovanni Tomaselli,[1] Tomás Muñoz Santoro,[2] Piersandro Pallavicini,[1] Carlos Ortiz de Solorzano,[2] Yuri Antonio Diaz Fernandez[1,*]

Affiliations:

[1] inLAB, Department of Chemistry, University of Pavia, Via Taramelli 12, Pavia, 27100, Italy

[2] Program in Biomedical Engineering. CIMA Universidad de Navarra, Cancer Center Clínica Universidad de Navarra (CCUN), Pamplona, Spain.

* corresponding author: ydf@unipv.it

[a] These authors contributed equally to this work.

SI 1 Kinetic stability data of the liposomes

Table SI1 Key quality attributes of the liposomes freshly prepared and after 6 weeks. Average MADLS size, backDLS size, polydispersity index (PDI) and particle number concentration.

	LP50		**LP100**		**LP200**		**LP400**	
	T_0	**T_{6weeks}**	**T_0**	**T_{6weeks}**	**T_0**	**T_{6weeks}**	**T_0**	**T_{6weeks}**
MADLS Size (nm)*	121±2	125±4	167±1	175±5	228±2	250±12	440±13	438±9
backDLS size (nm)*	119±3	117.0±0.7	164.2±0.7	164±3	225±4	227±4	380±10	373±5
PDI*	0.04 ±0.03	0.06 ±0.03	0.037 ±0.006	0.04 ±0.02	0.037 ±0.006	0.14 ±0.01	0.12 ±0.05	0.14 ±0.01
Particle Concentration ($x10^{10}$ particles/ml)	1.98 ±0.09	2.1 ±0.2	0.48 ±0.02	0.54 ±0.07	0.14 ±0.09	0.159 ±0.009	0.100 ±0.008	0.08 ±0.05

*Batch analysis data for 1 ml of 0.1 mg/ml liposomes. Shown data represents the average of three measurements

SI 2 Batch to bath variability for each liposome type

Table S2a Average MADLS size, backDLS size, polydispersity index (PDI), and particle number concentrations for the liposomes, ± standard deviations of three different preparation batches.

	Size (nm)	backDLS size (nm)	PDI	Particle Concentration ($X10^{10}$ particles/ml)
LP50	130±10	123±7	0.05±0.02	6±2
LP100	164±6	159±10	0.050±0.009	1.8±0.7
LP200	224±20	212±12	0.10±0.05	0.45±0.03
LP400	393±44	350±3	0.17±0.02	0.154±0.006

*Batch analysis data for 1 ml of 0.3 mg/ml liposomes. Shown data represent the average of three measurements.

SI 3 cryoTEM data processing and benchmark against DLS

Cryo TEM image processing

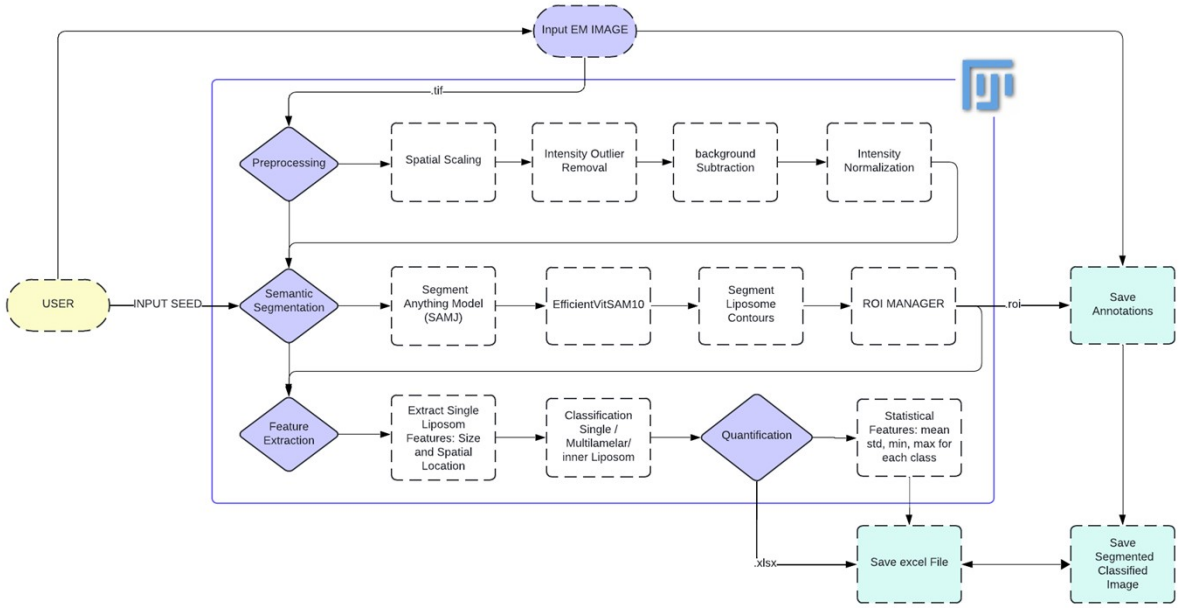

Figure SI3a Workflow for the supervised segmentation algorithm use for the analysis of liposomes size and structural features using cryoTEM images.

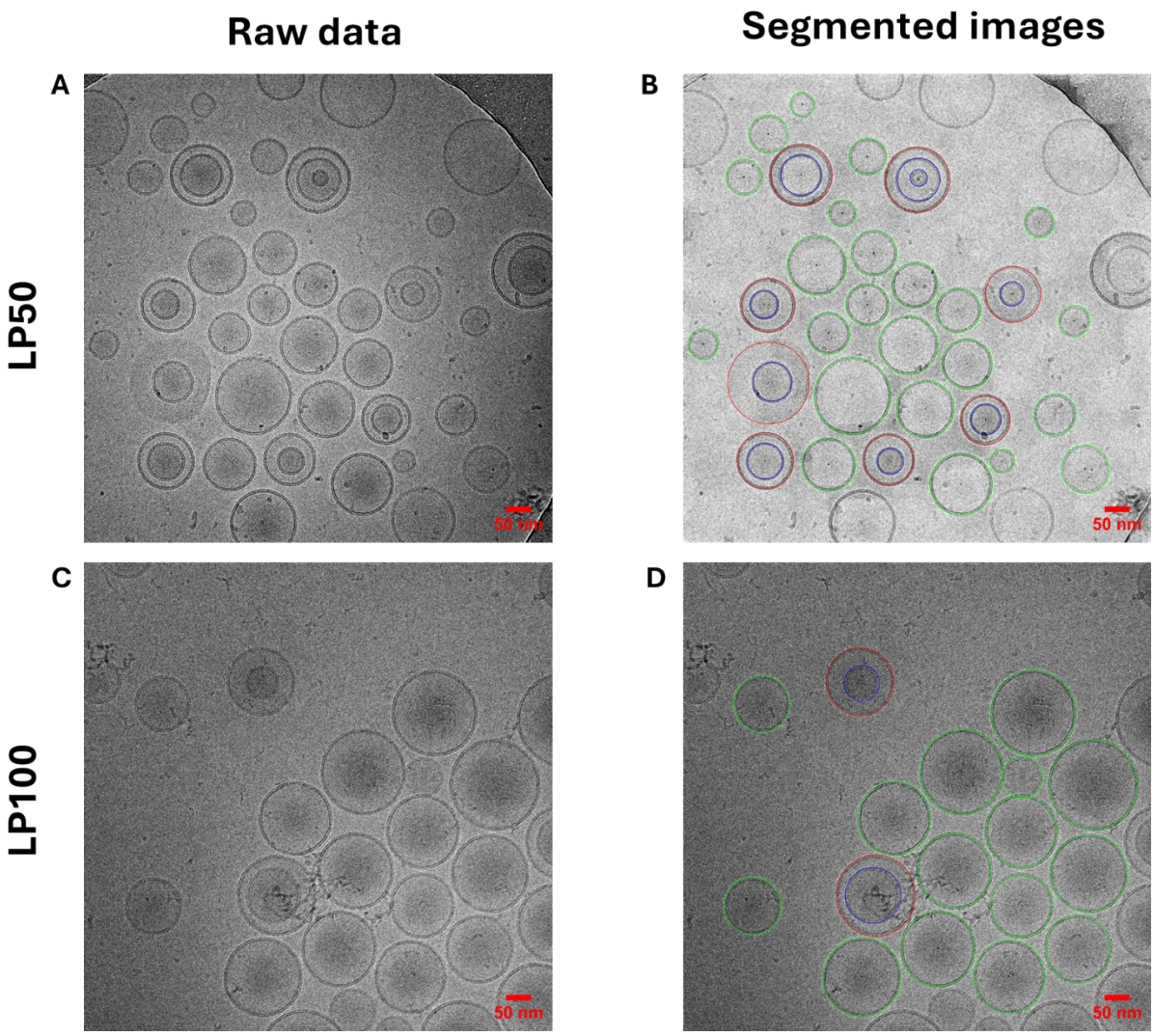

Figure SI3b Representative cryoTEM images before (left column) and after imaging processing (right column) for liposomes samples LP50 and LP100. Simple vesicles are identified and labelled in green, external lipid bilayer of multilamellar vesicles are labelled in red, and vesicles internalized are labelled in blue.

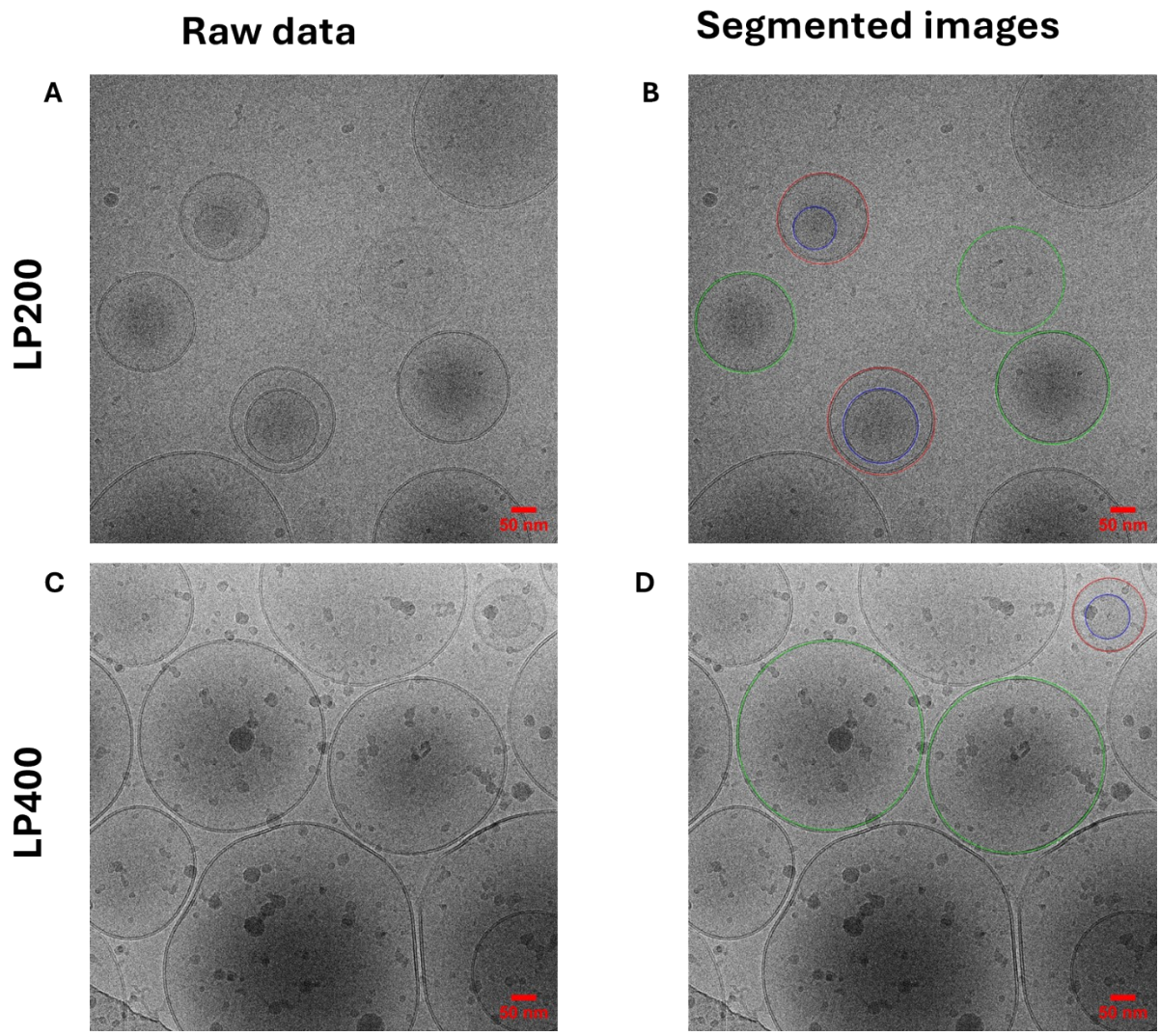

Figure SI3c Representative cryoTEM images before (left column) and after imaging processing (right column) for liposomes samples LP200 and LP400. Simple vesicles are identified and labelled in green, external lipid bilayer of multilamellar vesicles are labelled in red, and vesicles internalized are labelled in blue.

Benchmarking of DLS and cryoTEM data

Table SI3a- Z Test Matrix for LP50 Sizing (MADLS, BackDLS, TEM)

Z test LP50	MADLS	BackDLS	TEM
MADLS		1.04	0.76
BackDLS	1.04		0.70
TEM	0.76	0.70	

Table SI3b- Z Test Correlation Matrix for LP100 Sizing (MADLS, BackDLS, TEM)

Z test LP100	MADLS	BackDLS	TEM
MADLS		1.37	0.45
BackDLS	1.37		1.93
TEM	0.45	1.93	

Table SI3c- Z Test Matrix for LP200 Sizing (MADLS, BackDLS, TEM)

Z test LP200	MADLS	BackDLS	TEM
MADLS		2.80	2.11
BackDLS	2.80		1.53
TEM	2.11	1.53	

Table SI3d- Z Test Matrix for LP400 Sizing (MADLS, BackDLS, TEM)

Z test LP400	MADLS	BackDLS	TEM
MADLS		0.47	2.32
BackDLS	0.47		1.88
TEM	2.32	1.88	

All values were below the critical Z threshold, suggesting that the distributions are not significantly different.

Estimation the effect of multi-lamellarity on particle size

Table S3e- Estimation of Size Bias Due to Multi-lamellarity in liposomes using CryoTEM data

	CryoTEM size (nm)		
	Average	Multilamellarity correction	Multilamellarity bias estimation
LP50	98	99	1
LP100	142	146	4
LP200	168	175	7
LP400	281	299	18

SI 4 Optimization of AF4 methods

The optimization of the power decay method was conducted using liposomes with a nominal size of 100 nm (LP100), diluted to a total lipid concentration of 1 mg/ml, following the general approach suggested by Gigault at al[1]. Initially, we kept unvaried the injection+focus time at 3 minutes and the exponent of power decay at 0.1, while varying the crossflow rate from 0.3 ml/min to 0.5 ml/min. The resulting AF4-UV fractograms at λ=280nm are presented in Figure S4a. We decided to proceed with a crossflow rate of 0.4 ml/min due to its lower retention ratio and higher recovery (approximately 90%) compared to both 0.3 ml/min and 0.5 ml/min (approximately 75%).

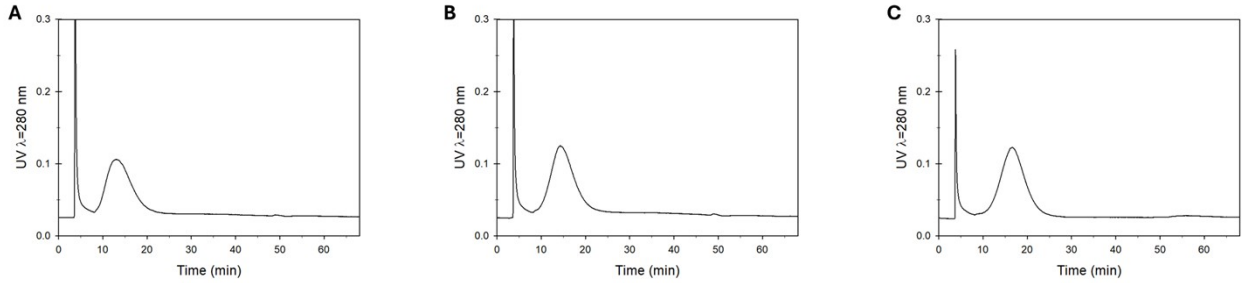

Figure S4a- AF4 UV fractograms (λ=280nm) of liposome LP100 1mg/mL analysed with power decay crossflow, injection+focus time at 3 minutes and exponent of power decay at 0.1, while varying the crossflow rate A) 0.3ml/min, B) 0.4ml/min and C) 0.5ml/min

Subsequently, we varied the focus+injection time to reduce the area of the void peak, testing injection times of 3, 7, and 10 minutes. As shown in Figure S4b, focus +injection time of 10 minutes lead to recoveries higher than 90% with the consequent decrease of the void peak area.

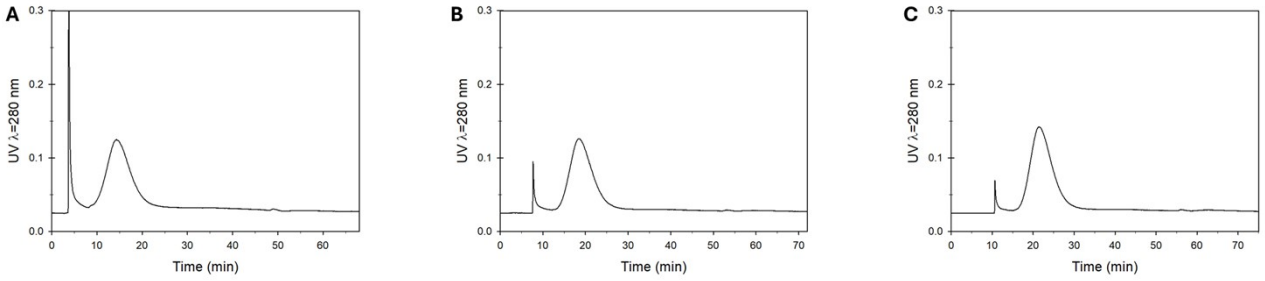

Figure S4b- AF4 UV fractograms (λ=280nm) of liposome LP100 1mg/mL analysed with power decay crossflow with exponent 0.1 and crossflow fixed at 0.4mg/min, while varying the injection+focus time A) 3 min, B) 7min and C) 10min.

Finally, we explored the exponent of power decay by testing values of 0.05, 0.1, and 0.2. The exponent of 0.1 lead to a recovery rate greater than 90% with high repeatability among replicates (standard deviation <5%), and therefore exponent 0.1 was chosen for the rest of experiments using the power decay method.

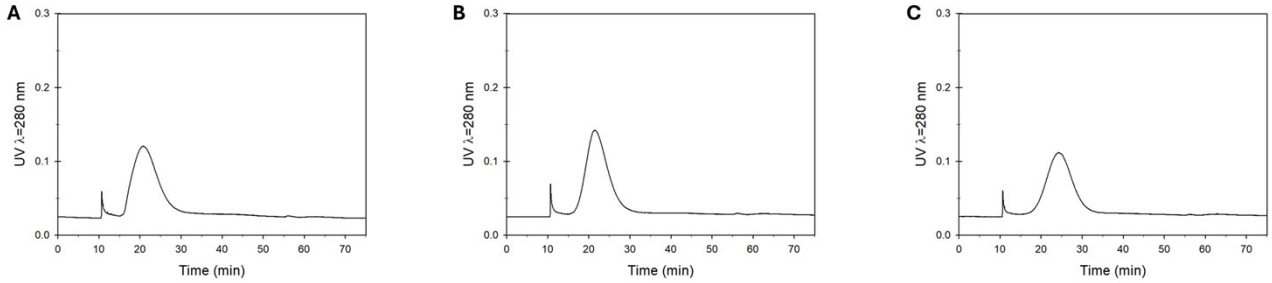

Figure 1- AF4 UV fractograms (λ=280nm) of liposome LP100 1mg/mL analysed with power decay crossflow injction+focus time fixed at 10 min and crossflow fixed at 0.4mg/min, while varying the exponent of power decay A) 0.05, B) 0.1 and C) 0.2.

We also optimized some key parameters for the constant crossflow method. We examined crossflow values ranging from 0.1 to 0.3ml/min, maintaining unaltered the other parameters at the values suggested by ASTM[2]; representative fractograms are shown in Figure S4c. The higher crossflow rate of 0.3 ml/min resulted in the complete elution of all liposomes by the end of the program only when the crossflow was switched off. To achieve satisfactory recovery at a crossflow rate of 0.2 ml/min, we had to extend the fractionation time due to the fact that elution times were longer and recoveries were low. The best results were obtained using a constant crossflow of 0.1 ml/min, providing good recovery and acceptable retention ratios [1,2].

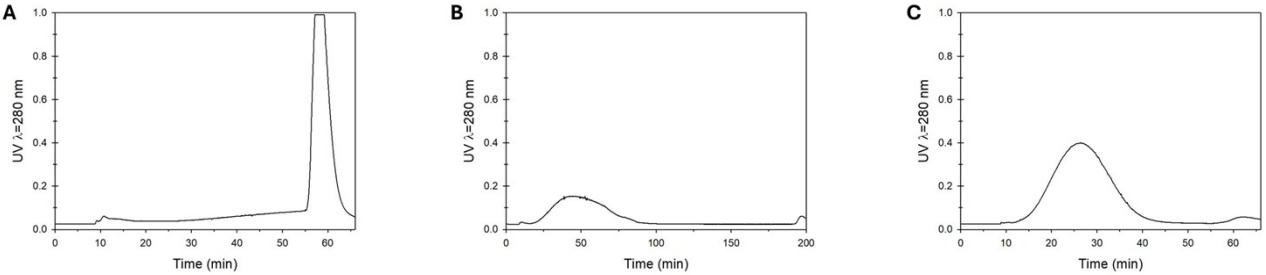

Figure S2c- AF4 UV fractograms (λ=280nm) of liposome LP100 1mg/mL analysed with constant crossflow with injection+focus time fixed at 8 minutes and varying the crossflow rate A) 0.3ml/min, B) 0.2ml/min and C) 015ml/min.

SI 5 Representative AF4 fractograms for the liposome systems and their key descriptors

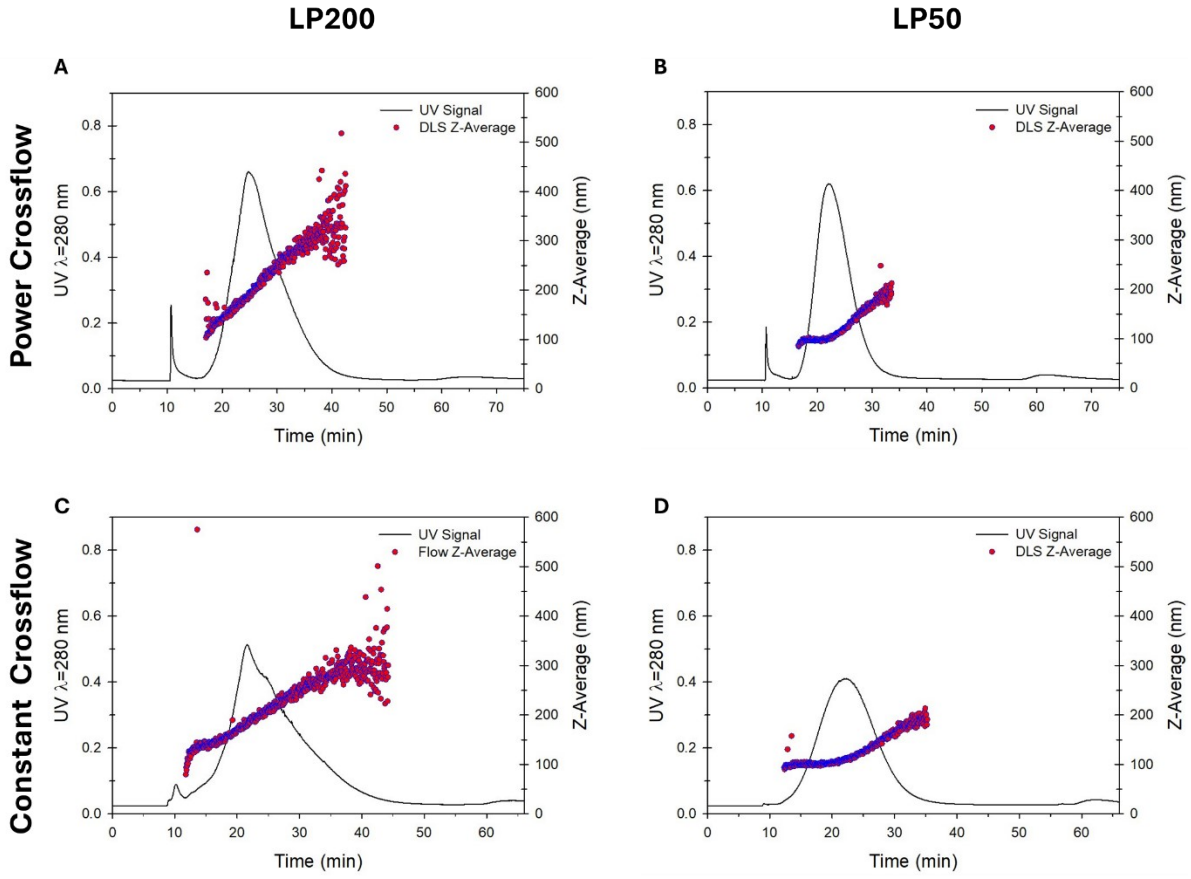

Figure SI5a Representative fractograms obtained by asymmetric flow field flow fractionation (AF4) for LP200 (A,C) and LP50 (B,D) using the power-decay crossflow method (first row) and the constant crossflow program (second row). Each plot shows the UV-Vis signal as a continuous line and the transient DLS Z-average diameter measured at 173° as a scatter plot. Data for LP100 and LP400 is presented in the main text.

Table SI5b Key fractogram descriptors for LP50, LP100, LP200 and LP400 with the two AF4 methods used in this work

LP50	Power Crossflow Method	Constant Crossflow Method
Recovery %	88±2	79±4
Relative void peak (min)	0.70±0.02	1.1549±0.0002
Relative retention time (min)	12.0±0.1	13.3±0.9
Retention Ratio	0.058±0.002	0.087±0.006
FWHM (min)	6.7±0.1	9.9±0.3
Full peak width (min)	16.8±0.2	22±1
Z-Average at MAX peak (nm)	101±1	109±3

LP100	Power Crossflow Method	Constant Crossflow Method
Recovery %	94.8±0.3	91±3
Relative void peak (min)	0.6834±0.0006	0.96±0.04
Relative retention time (min)	14.8±0.1	19.1±0.3
Retention Ratio	0.0462±0.0003	0.049±0.002
FWHM (min)	9.5±0.3	14.4±0.5
Full peak width (min)	21.7±0.4	32±1
Z-Average at MAX peak (nm)	130±2	147±6

LP200	Power Crossflow Method	Constant Crossflow Method
Recovery %	96±3	91±3
Relative void peak (min)	0.70±0.02	2.23±0.04
Relative retention time (min)	14.8±0.2	14.4±0.7
Retention Ratio	0.0470±0.0009	0.156±0.006
FWHM (min)	9.3±0.3	10.6±0.8
Full peak width (min)	25.6±0.2	32.8±0.6
Z-Average at MAX peak (nm)	192±3	194±4

LP400	Power Crossflow Method	Constant Crossflow Method
Recovery %	96±3	90±2
Relative void peak (min)	0.6836±0.0009	1.01±0.06
Relative retention time (min)	13.9±0.2	12.6±0.6
Retention Ratio	0.0491±0.0004	0.081±0.008
FWHM (min)	4.2±0.5	7.3±0.5
Full peak width (min)	29±2	42.8±0.6
Z-Average at MAX peak (nm)	248±7	287±6

FWHM: Full width half maximum

Repeatability of AF4 analysis for LP100

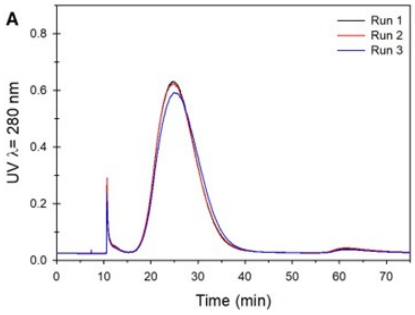

Run	Recovery %	Relative Void Peak (min)	Relative Retention Time (min)	Retention Ratio	Peak width (min)	Z-Average at MAX peak (nm)
1	95.1	0.6830	14.8	0.0462	21.4	128
2	94.8	0.6831	14.7	0.0464	21.7	130
3	94.6	0.6841	14.9	0.0459	22.1	132
Average	94.8±0.3	0.6834 ±0.0006	14.8±0.1	0.0462 ±0.0003	21.7±0.4	130±2

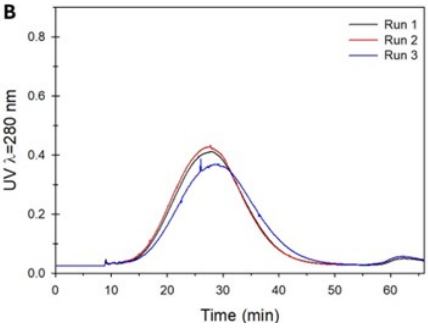

Run	Recovery %	Relative Void Peak (min)	Relative Retention Time (min)	Retention Ratio	Peak width (min)	Z-Average at MAX peak (nm)
1	90.9	1.0089	19.3	0.0510	31.3	150
2	94.0	0.9358	19.3	0.0474	32.4	150
3	87.6	0.9363	18.8	0.0486	33.5	140
Average	91±3	0.96 ±0.04	19.1±0.3	0.049 ±0.002	32±1	147±6

Repeatability of AF4 analysis for LP50

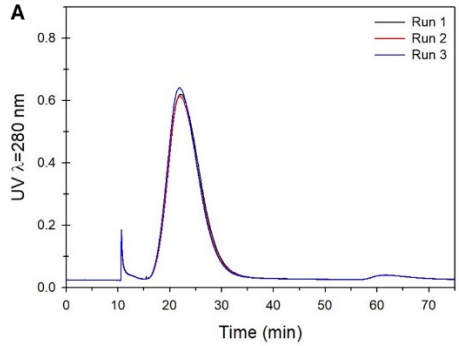

Run	Recovery %	Relative Void Peak (min)	Relative Retention Time (min)	Retention Ratio	Peak width (min)	Z-Average at MAX peak (nm)
1	89.5	0.6825	12.1	0.0565	17.0	100
2	85.6	0.7194	12.0	0.0601	16.8	102
3	89.0	0.6836	11.9	0.0575	16.6	101
Average	88±2	0.70 ±0.02	12.0±0.1	0.058 ±0.002	16.8±0.2	101±1

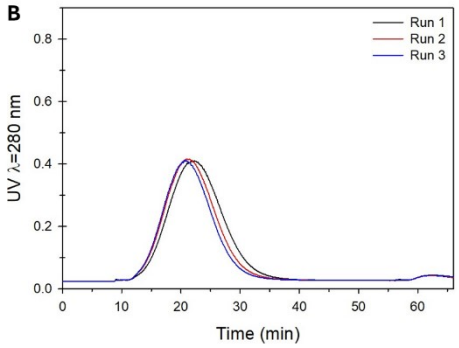

Run	Recovery %	Relative Void Peak (min)	Relative Retention Time (min)	Retention Ratio	Peak width (min)	Z-Average at MAX peak (nm)
1	82.8	1.1547	14.3	0.0808	23.0	112
2	78.8	1.1550	12.9	0.0897	21.5	108
3	74.7	1.1550	12.6	0.0915	20.6	106
Average	79±4	1.1549 ±0.0002	13.2±0.9	0.087 ±0.006	22±1	109±3

Repeatability of AF4 analysis for LP400

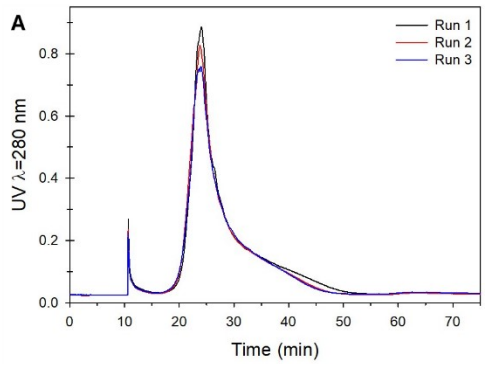

Run	Recovery %	Relative Void Peak (min)	Relative Retention Time (min)	Retention Ratio	Peak width (min)	Z-Average at MAX peak (nm)
1	99.6	0.6846	14.1	0.0487	30.7	242
2	96.0	0.6835	13.8	0.0496	28.0	255
3	92.9	0.6828	13.9	0.0490	27.8	247
Average	96±3	0.6836 ±0.0009	13.9±0.2	0.0491 ±0.0004	29±2	248±7

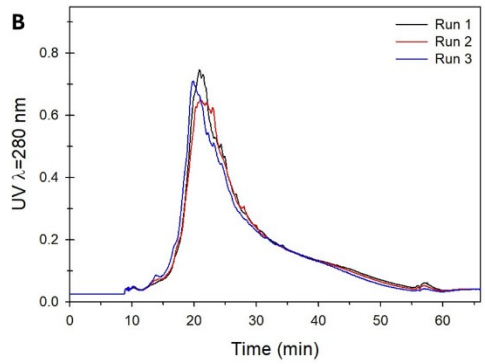

Run	Recovery %	Relative Void Peak (min)	Relative Retention Time (min)	Retention Ratio	Peak width (min)	Z-Average at MAX peak (nm)
1	92.2	1.0450	12.8	0.0814	43.0	287
2	88.9	0.9366	13.0	0.0721	43.2	293
3	89.6	1.0474	11.9	0.0883	42.1	282
Average	90±2	1.01 ±0.06	12.6±0.6	0.081 ±0.008	42.8±0.6	287±6

Repeatability of AF4 analysis for LP200

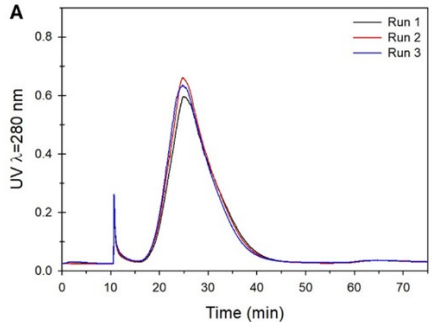

Run	Recovery %	Relative Void Peak (min)	Relative Retention Time (min)	Retention Ratio	Peak width (min)	Z-Average at MAX peak (nm)
1	92.5	0.7194	15.0	0.0480	25.8	195
2	98.3	0.6828	14.7	0.0466	25.5	190
3	95.9	0.6830	14.7	0.0464	25.6	190
Average	96±3	0.70±0.02	14.8±0.2	0.0470 ±0.0009	25.6±0.2	192±3

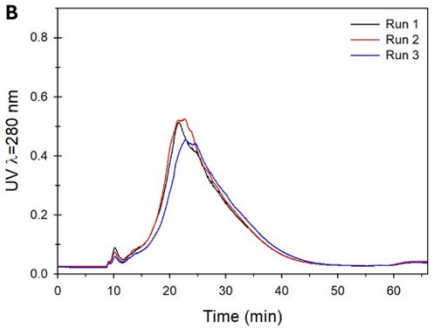

Run	Recovery %	Relative Void Peak (min)	Relative Retention Time (min)	Retention Ratio	Peak width (min)	Z-Average at MAX peak (nm)
1	89.7	2.2093	13.6	0.1624	32.4	190
2	94.2	2.210	14.7	0.1504	32.6	224
3	88.6	2.2825	14.8	0.1542	33.3	195
Average	91±3	2.23±0.04	14.4±0.7	0.156 ±0.006	32.8±0.5	203±18

SI6 Comparison of transient and batch DLS measurements

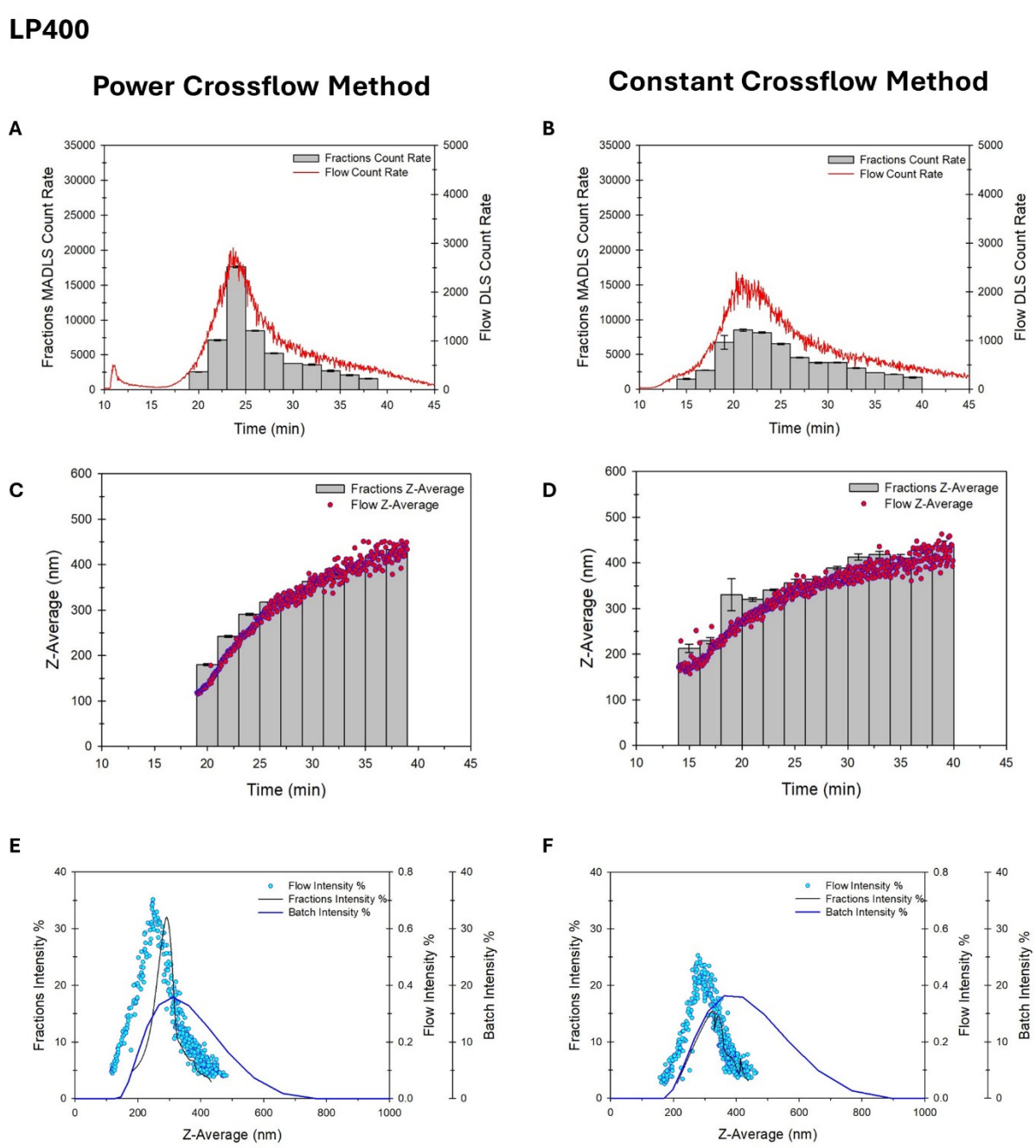

Figure S6a. Comparison of transient AF4-DLS and batch DLS on the fractions for LP400 using the power decay crossflow method (first column) and constant crossflow method (second column) for transient AF4 and collected fractions. A,B) DLS count rate as function of time. C,D) DLS Z-average diameter as a function of time. E,F) Comparison of transient AF4 size distributions in flow, size distributions obtained from the collected fractions, and original size distribution before fractionation.

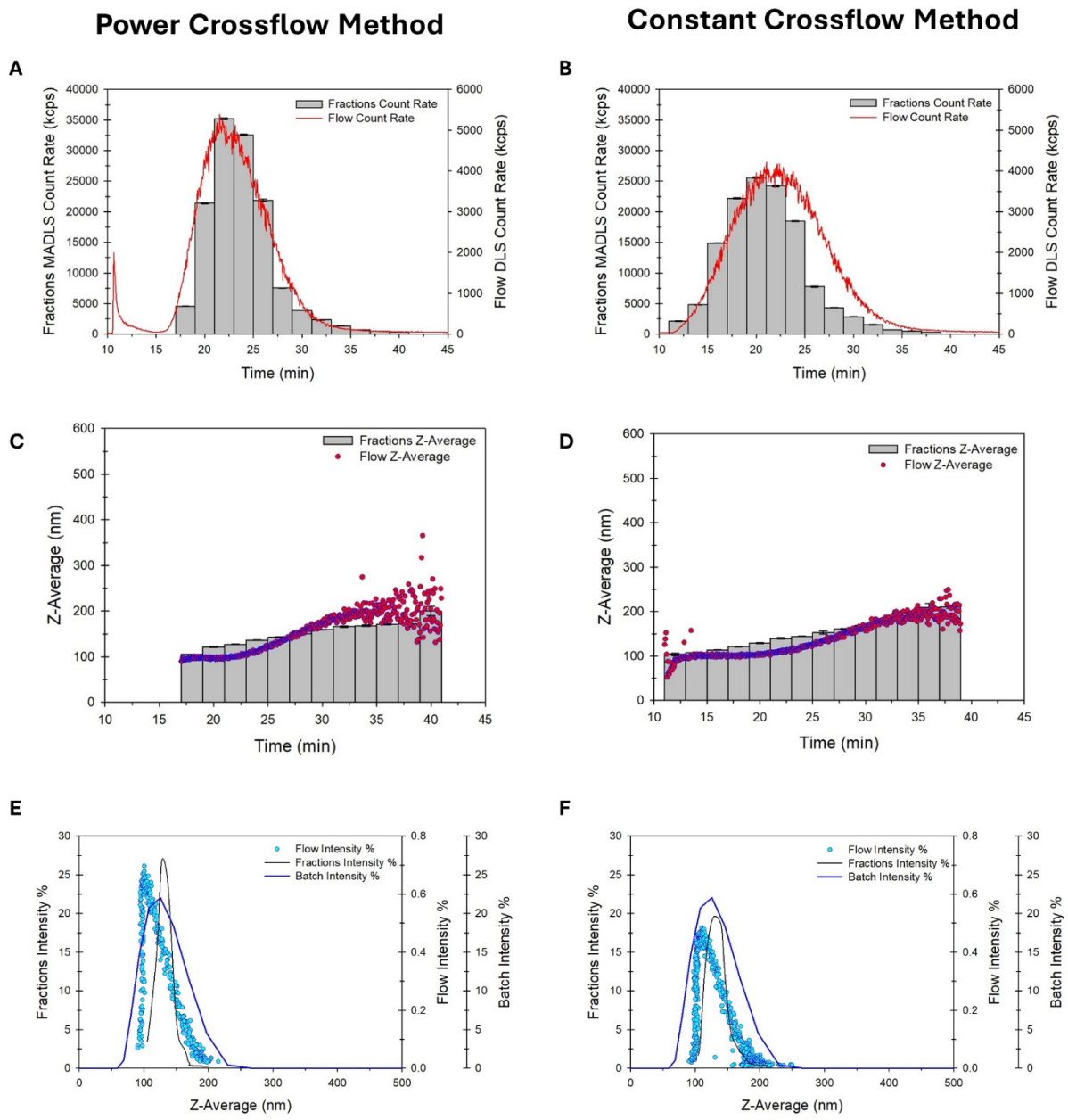

Figure S6b. Comparison of transient AF4-DLS and batch DLS on the fractions for LP50 using the power decay crossflow method (first column) and constant crossflow method (second column) for transient AF4 and collected fractions. A,B) DLS count rate as function of time. C,D) DLS Z-average diameter as a function of time. E,F) Comparison of transient AF4 size distributions in flow, size distributions obtained from the collected fractions, and original size distribution before fractionation.

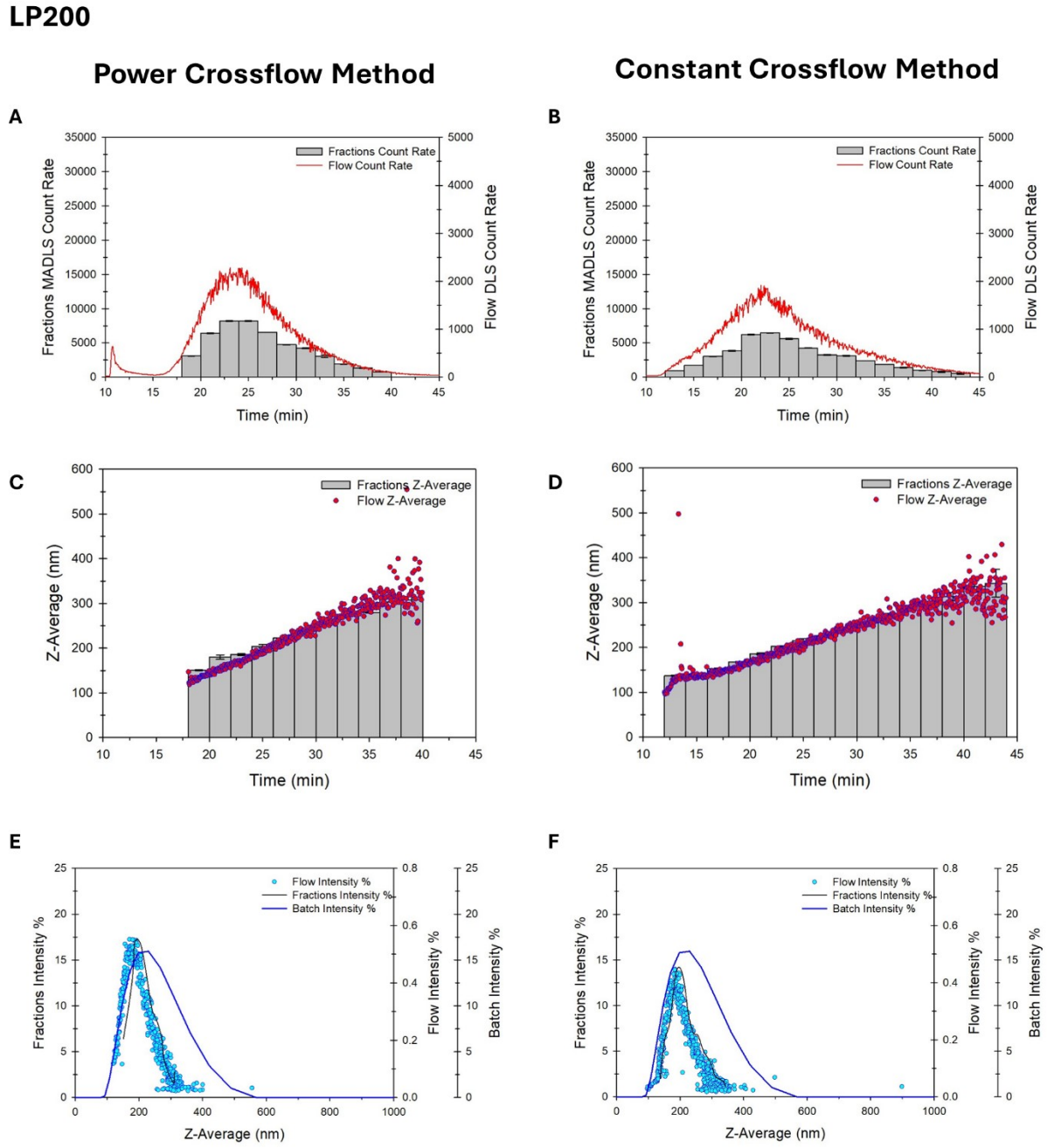

Figure S6c. Comparison of transient AF4-DLS and batch DLS on the fractions for LP200 using the power decay crossflow method (first column) and constant crossflow method (second column) for transient AF4 and collected fractions. A,B) DLS count rate as function of time. C,D) DLS Z-average diameter as a function of time. E,F) Comparison of transient AF4 size distributions in flow, size distributions obtained from the collected fractions, and original size distribution before fractionation.

SI7 Effect of particle concentration and detector flow on analytical bias for the determination of liposome size by AF4-DLS

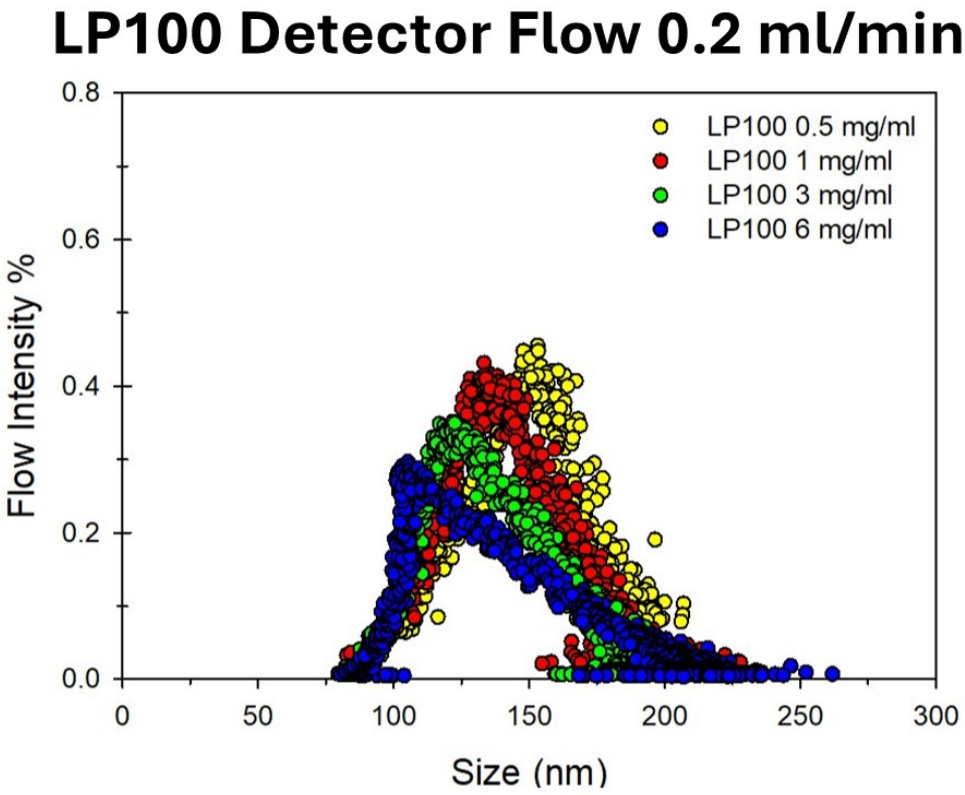

Figure SI7a. Effect of injected sample concentration on the transient AF4-DLS size distributions obtained with power-decay crossflow method for LP100

Table SI7b Comparison of the effect of two detector crossflow values (0.5 and 0.2ml/min) and different sample concentrations on size determination by AF4-DLS

			Flow Z-Average (nm)	
	Injected sample concentration	Batch backDLS size (nm)	**Detector Flow 0.5 ml/min**	**Detector Flow 0.2 ml/min**
LP100	6 mg/ml	152.7±0.9	124	121
	3 mg/ml		134	130
	1 mg/ml		145	140
	0.5 mg/ml		147	148

SI 8 Correlation coefficients between analytical bias in size determination and DLS data

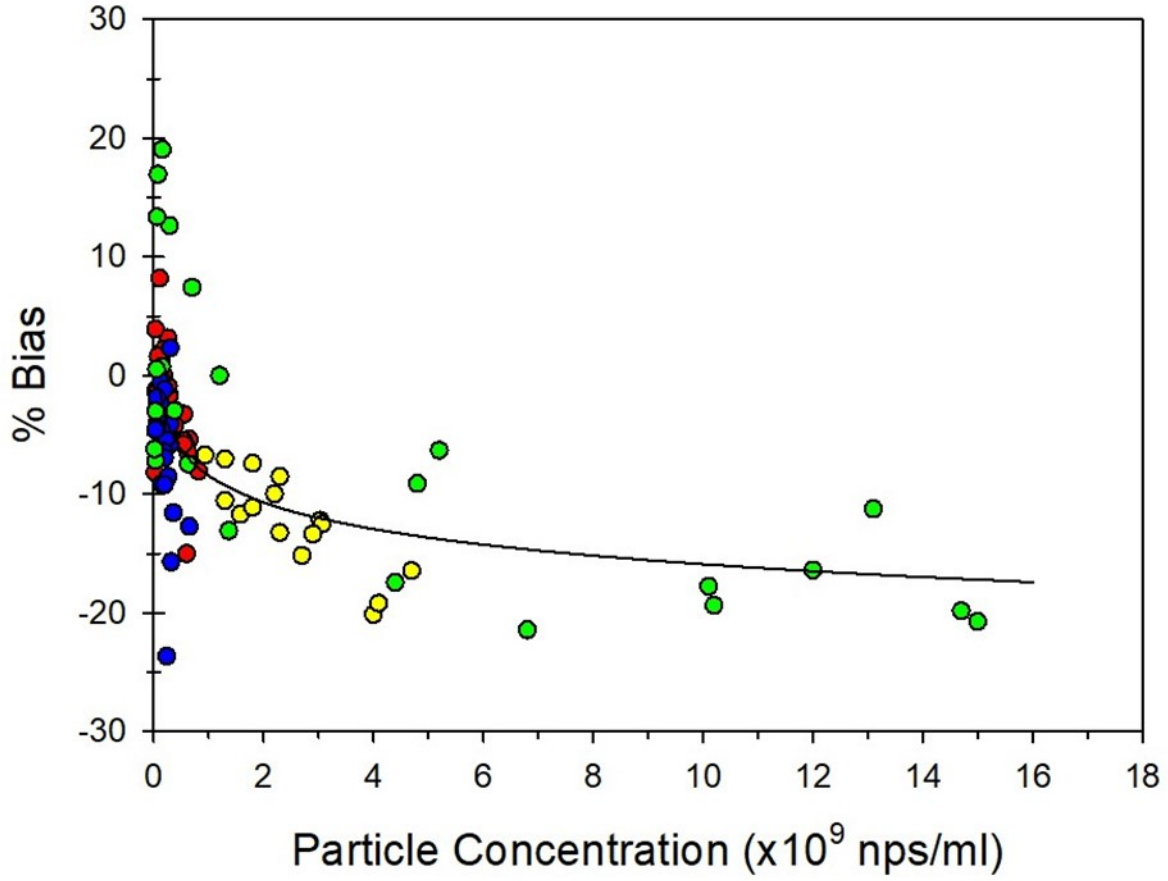

Figure SI8a Correlograms of the relative bias (%Bias) on the determination of average size by AF4-DLS and particle number concentration of the collected fractions. Each combination of sample type and AF4 method is plotted on a different color. The solid line is an empirical non-linear fitting.

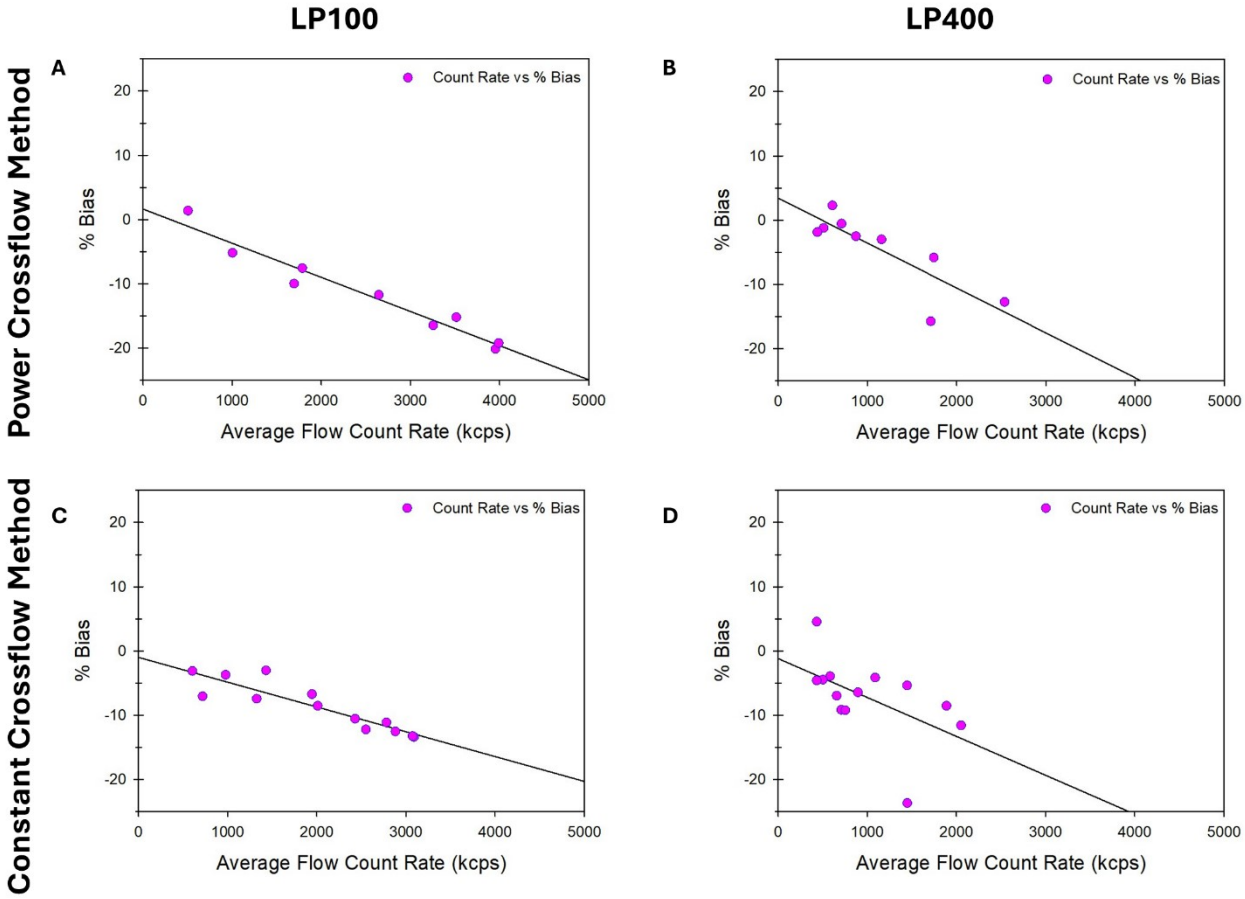

Figure SI8b Representative correlograms of the transient count rate at the DLS detector and relative bias on the determination of average size by AF4-DLS for LP100 and LP400

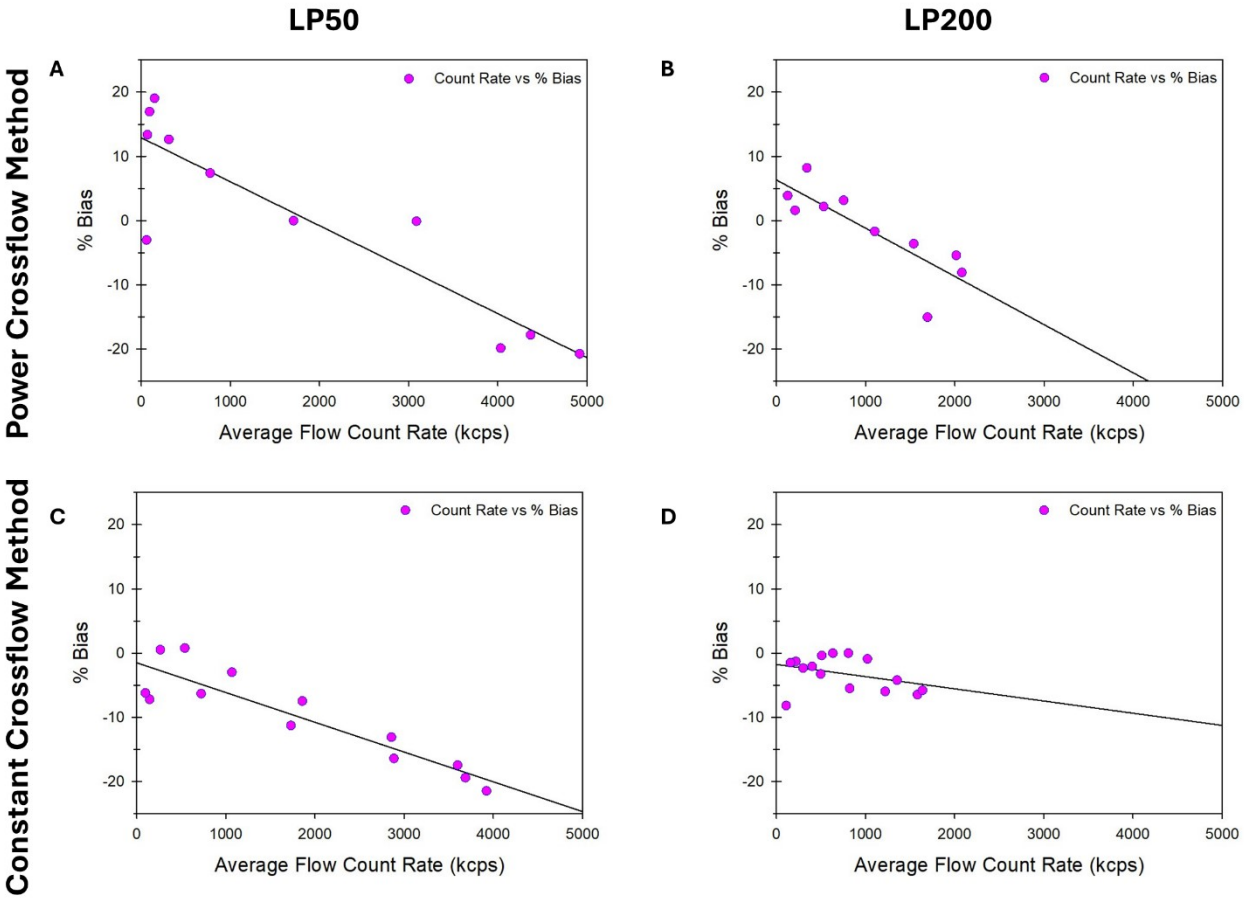

Figure SI8c Representative correlograms of the transient count rate at the DLS detector and relative bias on the determination of average size by AF4-DLS for LP50 and LP200

SI9-Characterization of polymeric nanoparticles:

Table 9- Key quality attributes of polymeric nanoparticles used in this work measured by multiangle dynamic (MADLS) and dynamic light scattering at angle 173° (backDLS).

	PS	**PMMA**
MADLS Size (nm)	69.95	114.1
backDLS size (nm)*	71.2±0.4	122±2
PDI*	0.022±0.006	0.10±0.03
Z-Potential (mV)*	-28±3	-39±4

SI 10 Representative AF4 fractograms for PS and PMMA nanoparticle and their key descriptors

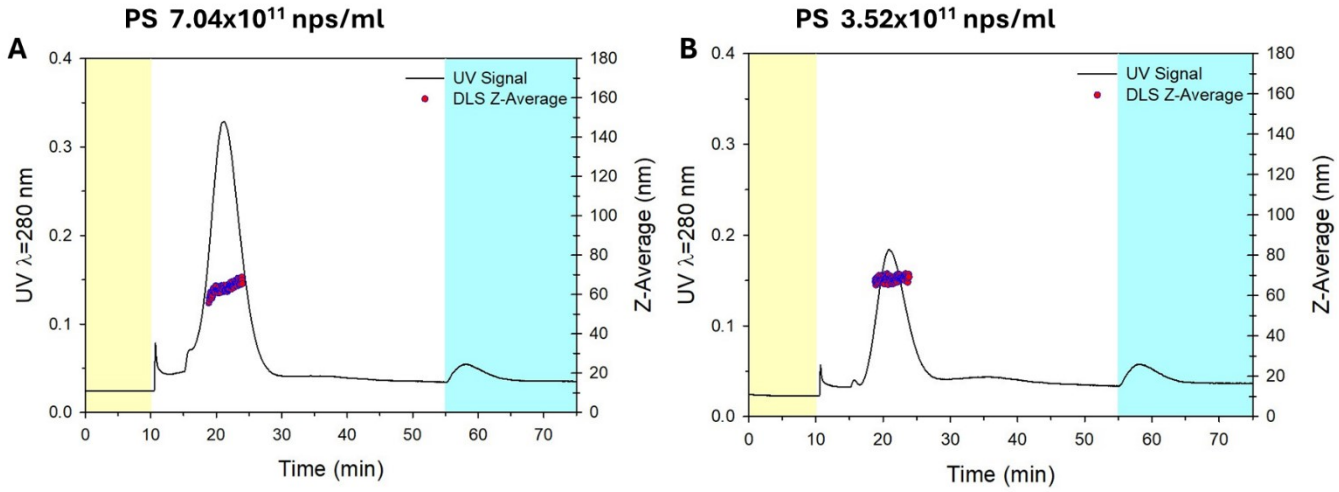

Figure SI10a- Representative fractograms obtained by asymmetric flow field flow fractionation (AF4) for PS nps using the power-decay crossflow Each plot shows the UV-Vis signal as a continuous line and the transient DLS Z-average diameter measured at 173° as a scatter plot. Yellow time zones represent the AF4 focusing and blue time zones indicate elution at zero crossflow.

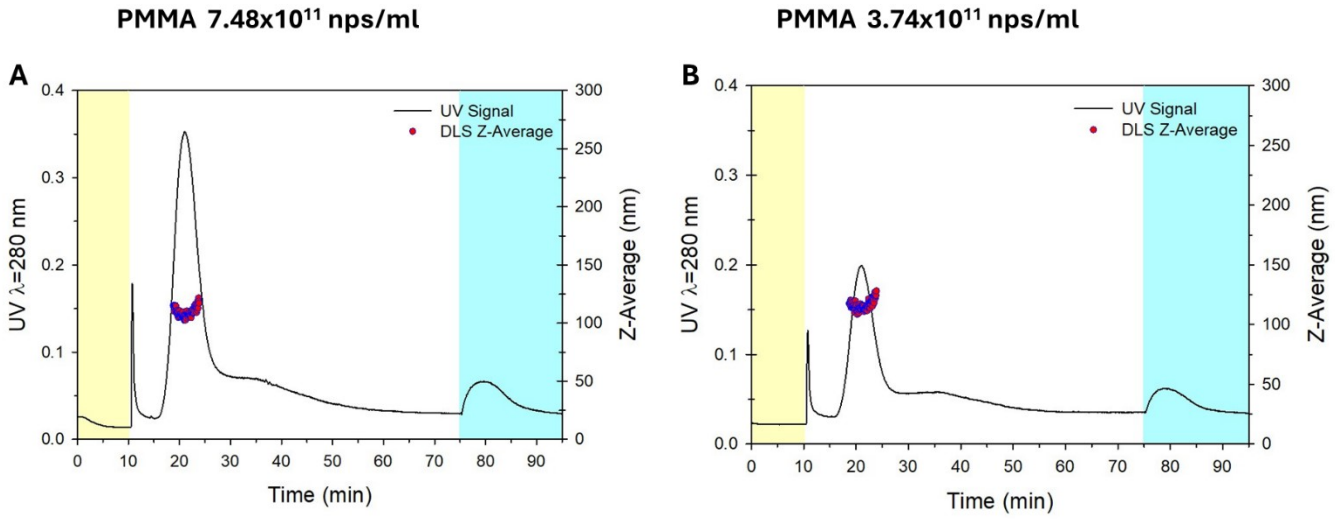

Figure SI10b- Representative fractograms obtained by asymmetric flow field flow fractionation (AF4) for PMMA nps using the power-decay crossflow Each plot shows the UV-Vis signal as a continuous line and the transient DLS Z-average diameter measured at 173° as a scatter plot. Yellow time zones represent the AF4 focusing and blue time zones indicate elution at zero crossflow.

SI11- Concentration-Dependent Size Behavior of Polymeric Nanoparticles Analyzed by AF4-DLS

Table SI10- Effect of injected sample concentration on the average size of the polymeric nanoparticles (PS and PMMA) calculated by transient AF4-DLS in-flow

	backDLS size (nm)	Injected sample concentration ($x10^{11}$ nps/ml)	Flow Z-Average (nm)	% Bias
PS	71.2±0.4	17.6	58	-18.5
		14.1	59	-17.1
		7.04	63	-11.5
		3.52	68	-4.5
PMMA	122±2	22.4	89	-27.0
		11.2	103	-15.5
		7.48	109	-10.5
		3.74	116	-4.8

SI12 Theoretical estimation of the effect of multiple scattering on size measurements by DLS

As discussed in the relevant section of the main text, DLS measurements rely on the determination of the time-dependent intensity autocorrelation function in a dynamic regime dominated by the Brownian motion of the particles and by the presence of single scattering events across the population of particles probed. It is reasonable to assume that at higher particle concentrations the likelihood for a photon to encounter multiple scatters before reaching the detector will be increased, leading to an artificially faster decay of the autocorrelation function and to an effective reduction of the measured particle size.[3]

The average number of single scattering events ($\bar{n}$) will depend on the scattering cross section of the single particles (σ) according to the expression[4]:

$$\bar{n} = \sigma \cdot C_{NP} \cdot l \qquad \text{Eq.S1}$$

Where C_{NP} is the particle number concentration of the scatterers and l is the characteristic length of the probing volume. If we assume that multiple scattering is the result of two independent scattering events under a photon efflux ϕ, the average number for multiple-scattered photons ($\bar{m}$) can be written:

$$\bar{m} \approx \frac{(\bar{n})^2}{\phi} \qquad \text{Eq.S2}$$

Furthermore, if we interpret the effect of multiple scattering on the autocorrelation function as a virtual population of scatterers with a characteristic particle size d_m different from the actual particle size d derived from single scattering events, the average size measured experimentally (d_{exp}) in the presence of multiple scattering could be estimated by the expression:

$$d_{exp} = \frac{\bar{n} \cdot d + \bar{m} \cdot d_m}{\bar{n} + \bar{m}} \qquad \text{Eq.S3}$$

Substituting Eq.S1 and Eq.S2 in Eq.S3 and simplifying the terms we obtain:

$$d_{exp} \approx \frac{d + \left(\frac{\sigma \cdot C_{NP} \cdot l}{\phi}\right) \cdot d_m}{1 + \frac{\sigma \cdot C_{NP} \cdot l}{\phi}} \qquad \text{Eq.S4}$$

And considering $\frac{\sigma \cdot C_{NP} \cdot l}{\phi} \ll 1$ in Eq.S4, we derived a direct expression for the analytical bias on size determination:

$$\%Bias = \frac{d - d_{exp}}{d} \cdot 100 \approx \; -\left(\frac{\sigma \cdot C_{NP} \cdot l}{\phi}\right) \cdot \frac{d_m}{d} \cdot 100$$

Eq.S5

This expression can be further rationalized if we account for the assumption that d_m is a function of the probability of multiple scattering $\left(\frac{\bar{m}}{\phi}\right)$ and can be expanded in series:

$$d_m = d - a \cdot \frac{\bar{m}}{\phi} + o\left[\left(\frac{\bar{m}}{\phi}\right)^2\right]$$

Eq.S6

Substituting Eq.S6 and Eq.S2 into Eq.S5 and considering the we can write:

$$\%Bias \approx \; -\left(\frac{\sigma \cdot C_{NP} \cdot l}{\phi}\right) \cdot \left[1 - \frac{a}{d} \cdot \left(\frac{\sigma \cdot C_{NP} \cdot l}{\phi}\right)\right] \cdot 100$$

Eq.S7

And considering again $\frac{\sigma \cdot C_{NP} \cdot l}{\phi} \ll 1$, Eq.S7 reduces to:

$$\%Bias \approx \; -\left(\frac{\sigma \cdot C_{NP} \cdot l}{\phi}\right) \cdot 100$$

Eq.S8

It is relevant to note that the term within brackets in Eq.S8 is the probability for single scattering, that will be proportional to the count rate for scattering intensity, explaining the linear relationship between %Bias and DLS measured count rate, independently of the size and chemical composition of the particles analyzed.

Bibliography for Supporting information

1 J. Gigault, J. M. Pettibone, C. Schmitt and V. A. Hackley, *Anal. Chim. Acta*, 2014, **809**, 9–24.

2 I. ASTM, *E3409-24*, 2024, 545-545–3.

3 R. Ragheb and U. Nobbmann, *Sci. Rep.*, 2020, **10**, 1–9.

4 C. M. Sorensen, R. C. Mockler and W. J. O'Sullivan, *Phys. Rev. A*, 1978, **17**, 2030–2035.